

UC Berkeley

UC Berkeley Previously Published Works

Title

Ion exchange selectivity in clay is controlled by nanoscale chemical-mechanical coupling

Permalink

<https://escholarship.org/uc/item/4rg8x4cc>

Journal

Proceedings of the National Academy of Sciences of the United States of America, 116(44)

ISSN

0027-8424

Authors

Whittaker, Michael L
Lammers, Laura N
Carrero, Sergio
[et al.](#)

Publication Date

2019-10-29

DOI

10.1073/pnas.1908086116

Supplemental Material

<https://escholarship.org/uc/item/4rg8x4cc#supplemental>

Peer reviewed

Ion exchange selectivity in clay is controlled by nanoscale chemical-mechanical coupling

Michael L. Whittaker,^{1,2} Laura N. Lammers,^{1,3} Sergio Carrero,^{1,2} Benjamin Gilbert,² Jillian F. Banfield^{1,2,3*}

¹ Energy Geosciences Division, Lawrence Berkeley National Laboratory, Berkeley, California, USA 94720.

² Department of Earth and Planetary Science, University of California, Berkeley, California, USA 94720.

³ Department of Environmental Science, Policy, and Management, University of California, Berkeley, California, USA 94720.

*To whom correspondence should be addressed jbansfield@berkeley.edu

Keywords: montmorillonite, ion exchange, dynamic equilibrium, cryo-TEM

Physical Sciences: Earth, Atmospheric and Planetary Sciences

Ion exchange in nanoporous clay-rich media plays an integral role in water, nutrient, and contaminant storage and transport. In montmorillonite (MMT), a common clay mineral in soils, sediments, and muds, the swelling and collapse of clay particles through the addition or removal of discrete molecular layers of water alters cation exchange selectivities in a poorly understood way. Here we show that ion exchange is coupled to the dynamic delamination and restacking of clay layers, which creates a feedback between the hydration state of the exchanging cation and the composition of the clay interlayer. Particles with different hydration states are distinct phases with unique binding selectivities. Surprisingly, equilibrium achieved through thermal fluctuations in cation concentration and hydration state leads to the exchange of both ions and individual MMT layers between particles, a process we image directly with high-resolution cryo-TEM. We introduce an exchange model that accounts for the binding selectivities of different phases, which is likely applicable to many charged colloidal or macromolecular systems in which the structural conformation is correlated with the activities of water and counterions within spatially confined compartments.

Significance. We directly visualize hydrated clay with near-atomic resolution and find that potassium and sodium bind in different configurations that result in distinct free energies. The way in which these ions bind affects the structure of the clay, which in turn changes the binding selectivity, creating a feedback that is not accounted for in current exchange models. We find that clay minerals can be far more dynamic than previously envisioned, and that rapid fluctuations may have long-term consequences for the fate of ions in clay-rich environments.

Clay minerals are by far the most abundant inorganic nanomaterial in the lithosphere.(1) As nanomaterials, their properties are very sensitive to the microscopic details of particle arrangements. Changes to the structure of clay minerals may have environmental-scale impacts because swelling clays (smectites) like MMT can control the rheological and mechanical properties of soils, sediments, and muds,(2) and the transport of solutes through them.(3)

The structures of smectites arise from molecular-scale interactions between 2:1 aluminosilicate layers, the counterions that balance charge arising from isomorphic substitutions within the layers, and associated waters of hydration (Fig. 1). Variation in the types and proportions of interlayer species causes face-to-face stacks of 2:1 layers of MMT to expand or collapse reversibly.(4, 5) Despite the importance of ion exchange in many environmental and geological systems containing

smectites, current models poorly describe the feedbacks between solution composition, ion exchange and interlayer swelling state that determine pore structure and macroscopic transport.

A challenge for developing an improved understanding of ion exchange in confinement is that to date, neither computational nor experimental approaches have been able to directly access the timescales over which both exchange and swelling/collapse occur. Molecular dynamics simulations have produced free-energy relationships for a narrow range of solution conditions(2) but simulations are restricted to small system sizes and timescales. Experiments often probe equilibrium swelling states under a variety of conditions,(4) but have not directly captured the rapid process of exchange. Neither simulations nor experiments have been able to explore the impact of rotation, translation or bending of layers on ion exchange during swelling and collapse.

We use *in situ* time-resolved simultaneous small-, medium-, and wide-angle X-ray scattering (SAXS/MAXS/WAXS) to probe the dynamics of ion exchange upon rapid mixing of homoionic sodium- or potassium-MMT suspensions with solutions containing the opposite cation. Transmission electron microscopy at cryogenic conditions (cryo-TEM) of hydrated samples *in aqua* provides a complementary snapshot of particle arrangements with near-atomic resolution. Combined, both techniques establish a consistent framework for determining the thermodynamics of ion exchange and offer new insights into the molecular mechanisms underlying clay particle structures and dynamics.

Results

Static X-ray scattering. Hydrated MMT particle structures were investigated with static X-ray scattering, which was used as a standard for comparison to cryo-TEM images and as a basis set for the fitting of time-resolved X-ray scattering. Homoionic Wyoming montmorillonite (SWy-2) was resuspended in NaCl (1 M) or KCl (1 M) to a concentration of 20 mg/mL (herein called Na-MMT or K-MMT). SAXS/MAXS/WAXS were acquired simultaneously on three separate detectors.(6) K-MMT exhibited a larger basal spacing scattering vector ($q_{001} = 0.40 \text{ \AA}^{-1}$, 15.9 Å), compared to Na-MMT ($q_{001} = 0.33 \text{ \AA}^{-1}$, 19.0 Å), consistent with two and three molecular layers of interlayer water, respectively. Peak intensity at q_{001} of K-MMT was much lower than the intensity of Na-MMT ($I_{K-MMT}^{001} / I_{Na-MMT}^{001} = 0.28$) and was much broader (0.05 and 0.13 Å⁻¹ for Na-MMT and K-MMT, respectively, Fig. 1 and SI Appendix), indicating a larger deviation from the average interlayer spacing and a higher fraction of poorly-stacked layers in K-MMT.

Higher-order diffraction at $\ell \cdot q_{001}$, where ℓ is the integer diffraction order ($\ell = 2, 3, 4$, and 6 for Na-MMT

and $\ell = 3, 5$ for K-MMT), is an indication that the particles are homogeneous with no interstratification. Potassium resides in close proximity to, or partially within, the silicate sheets, while sodium ions reside both near the silicate sheet and ~ 2.5 Å to either side of the interlayer midplane, on average.(7) Electron density, ρ , profiles along the stacking direction are derived by inverse Fourier transformation of the 00ℓ structure factors. X-ray derived ρ profiles are largely consistent with contrast profiles measured directly from low-dose cryo-TEM images (discussed below) and qualitatively agree with molecular models, which suggest that potassium makes inner-sphere complexes with ditrigonal cavities in the silicate sheet,(8) while the more tightly bound hydration shell of sodium increases its probability of residence near the interlayer midplane (Fig. 1c, f).(9) However, ρ profiles obtained from direct imaging indicate that sodium resides in close proximity to the basal surface with a higher frequency than expected from simulations or X-ray scattering. This is likely because transformation of reciprocal-space data does not account for peak width and asymmetry. Similarly, interlayer potassium may exhibit greater deviations from its average position than expected from X-ray scattering.

Time-resolved X-ray scattering. Ion exchange was performed by mixing a KCl solution (1 M) with Na-MMT in a stopped-flow mixer at four volume ratios, r , where $r = [K^+]/[Na^+]$: 2, 1, 0.5, and 0.33. After mixing with KCl the Na-MMT basal spacing peak at 19.0 Å decreased in intensity and a separate peak at 15.9 Å emerged (Fig. 2a). Two distinct peaks were clearly resolved in all cases and fitting confirmed that the peak positions did not change appreciably during exchange. This is a strong indication that the collapse front within an interlayer region is sharp and/or moves rapidly on the timescale of the measurements (~ 50 ms acquisition time). A single broadened peak with a maximum between the homoionic end-members was not observed under any *in situ* conditions in this study, excluding the possibility of extensive interstratification of collapsed and un-collapsed interlayers,(10) in agreement with cryo-TEM observations (below).

Ion exchange proceeded much more rapidly than collapse and swelling. While the $\ell = 2$ peak intensity for Na-MMT was approximately 4% of the $\ell = 1$ intensity at equilibrium (SI Appendix), the intensity dropped significantly after the first acquisition following mixing. The total noise level in the $\ell = 2$ region ($0.56 < q < 0.76$ Å⁻¹) after mixing was far less (by a factor of 2.7 - 9.6) than the intensity expected in this region by taking 4% of the 19 Å peak intensity, such that this peak would be resolved if present. Weak intensity in this region that fades after the first acquisition was often observed in such cases, even

when collapse did not go to completion, an indication of interlayer cation mixing.

The collapse rate was quantified using the integrated intensity from the basal spacing peaks (Fig. 2b), expressed as the instantaneous fraction of the 19-Å hydrate, $f(t)$, from

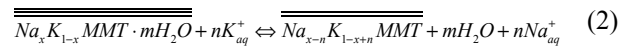
$$f(t) = \frac{I_{Na-MMT}^{001}}{I_{Na-MMT}^{001} + I_{K-MMT}^{001}} = (1 - f)e^{-at} + f \quad (1)$$

where $f = f(t \rightarrow \infty)$ is assumed to represent equilibrium, and a is a chemical-mechanical rate constant. The total intensity from both peaks decreases during exchange, even when accounting for particle dilution, while the total clay scattering signal remains constant. This requires that the total coherent scattering volume decreases as collapse progresses and therefore that particles must rearrange into configurations that scatter less strongly during collapse.

Both f and a were strong functions of the potassium concentration, but neither exhibited a strong temperature dependence (SI Appendix). This behavior contrasts with ion diffusion-limited exchange in anhydrous phyllosilicates,(11) which increases appreciably with temperature through the Arrhenius behavior of the diffusion coefficient.(12) Interlayer water diffusion has a strong temperature dependence,(13) while species exchange, including water, between bulk solution and the interlayer is essentially barrierless,(14, 15) indicating that neither process limits collapse.

These data are consistent with a dynamic equilibrium between two populations of particles(16-19) in a ratio that is determined by the solution composition. Current models of ion exchange equilibria in smectites,(20-23) do not account for the discrete equilibria between distinct hydration states and do not incorporate the change in water activity at each hydration state. However, it is known that the hydration state significantly alters ion binding selectivity. Therefore, we introduce a new model to account for these observations.

Thermodynamic exchange model. Ion exchange equilibrium between three-water-layer MMT ($\overline{\overline{\overline{MMT}}}$), two-water-layer MMT ($\overline{\overline{MMT}}$), and bulk aqueous solution can be expressed as



with x establishing the fraction of cation sites occupied by sodium, m water molecules released upon collapse, and n cations exchanged, per unit of structural charge. The law of mass action defines the equilibrium constant, K_{eq} , for this reaction as

$$K_{eq} = \left(\frac{Na^+}{K^+}\right)^n \alpha_w^m \frac{\overline{\overline{\overline{Na(x-n)K(1-x+n)MMT}}}}{\overline{\overline{Na_x K_{(1-x)} MMT}} \cdot mH_2O} \quad (3)$$

where quantities in parentheses refer to activities and a_w is the activity of water. Commonly reported values of interlayer water density (24, 25) give $m \cong 10$. Thus, the composition of the solid phases, which must obey $n \leq x$, can be constrained to the range $69 < x < 1$ (SI Appendix). This establishes the unique chemical composition of each collapse state. The standard Gibbs free energy, ΔG° , can be determined from K_{eq} such that $\Delta G^\circ < 4.2$ kT. This confirms that two- and three-water-layer hydrates are separate coexisting phases in equilibrium and separated by a difference in free energy that allows spontaneous interconversion via the thermal energy (SI Appendix). This model was extended over a range of sodium and potassium concentrations, allowing for the determination of a complete composition-phase diagram (Fig. 2c; SI Appendix for detail).

Low-dose cryogenic transmission electron microscopy. High resolution images of interlayer structure of single Na-MMT and K-MMT layers and basal spacing of particles (Fig. 3) confirm that they are distinct phases. Contrast profiles measured parallel to the stacking direction were in agreement with the electron density profiles calculated from X-ray scattering basal spacing peak intensities (Fig. 1b, e). Although layers were oriented edge-on with respect to the beam direction, Na-MMT layers were rarely also aligned along a high-symmetry zone axis and thus have no appreciable contrast variation within the layer (Fig. 3a). By chance, some Na-MMT layers were oriented along a high-symmetry axis, but these layers had no special orientational relationship with their neighbors (SI Appendix). This is consistent with turbostratic stacking commonly observed for MMT.

However, many K-MMT particles exhibited intraparticle lattice fringes that maintained correlated orientations across multiple neighboring layers (Fig. 3b-h). Enlargement of a region containing only two unit cells of MMT in each layer (Fig. 3c, e, g) revealed contrast that is entirely consistent with atomic models of MMT viewed along three high-symmetry crystallographic axes (Fig. 3d, f, h). Based on the expected angle at which the atomic potentials make and the cation-cation separation when viewed edge-on, each layer was uniquely attributed to $\langle 100 \rangle$, $\langle 110 \rangle$ or $\langle \bar{1} 10 \rangle$ zone axis.

Most Na-MMT particles had an average of 4.4 layers and were mostly coplanar, even preserving their spacing across gently deformed regions, while K-MMT particles had only 2.5 layers on average and were often twisted and bent (SI Appendix). This is consistent with lower X-ray scattering basal spacing peak intensity (Fig. 1d) and along with the observation of decreasing total basal spacing intensity in X-ray scattering during collapse in the presence of potassium, indicates that the MMT particles undergo delamination as a consequence of the ion exchange process.

Particles in $r = 0.5$ mixtures exhibited partially delaminated domains consisting of more than one layer not in contact with adjacent layers along their entire length due to local bending (SI Appendix). Because these images are taken from a time point (>10 s) well after the initial collapse (1-2 s), this is strong circumstantial evidence confirming that particles delaminate. Moreover, it also suggests that individual layers dynamically restack at equilibrium, since layers were not found to be completely delaminated.

Two distinct populations of particles exhibited either ~ 16 Å or ~ 19 Å interlayer spacings in cryo-TEM images (SI Appendix), also in agreement with SAXS data. Average interlayer spacings were determined from integrated FTs from 8 different particles comprising a total of 81 layers (over 10^4 nm total layer length with 0.074 nm pixel width, for a total of over 10^6 observations). Two particles (30 layers) retained ~ 19 Å spacing, while 6 particles (51 layers) were collapsed and had an average of ~ 16 Å interlayer spacing. The fraction of collapsed layers ($30/81 = 37\%$) is comparable to f at this composition measured from X-ray scattering ($48 \pm 8\%$, Fig. 2b) given the underrepresentation of K-MMT from X-ray scattering on a per-layer basis.

Discussion

Summary of geochemical model. Ion exchange of potassium for sodium in MMT causes phase separation, resulting in two populations of particles that are non-interstratified and chemically homogeneous. Each has a distinct cation selectivity that is determined by its hydration state and separated by approximately 4 kT. We show direct evidence that layers delaminate after potassium is introduced and suggest that this provides a mechanism for the spatial segregation of regions of different ion selectivities (i.e., different collapse states) and enables Brownian motion that promotes re-attachment at (near) crystallographic orientations.

Both phase-separated two- and three-water-layer interlayers are in dynamic equilibrium at an abundance (i.e., f) that is determined by the cation ratio in solution and the water activity. The observed end-member structures (Fig. 1) correspond to local minima in free energy in homoionic solutions.(8, 26) that are determined largely by cation hydration energies.(27, 28) Thus, we introduce an equilibrium model in which ion exchange drives changes in interlayer hydration state.

Beyond determining selectivity coefficients of multicomponent electrolytes that depend on the swelling state, this thermodynamic model can be used in the prediction of swelling pressures or volumetric strain associated with chemical perturbations in smectite-rich materials.(29) For example, it predicts higher swelling pressures in lower bulk K/Na clays due to increased swelling free energies. Swelling state distributions in high dry bulk density compacted clays are expected to favor

more collapsed states due to the decreased activity of water. However, the model only accounts for uniaxial pressure normal to the stacking direction and it does not capture the effects counterion composition on average particle size.

Chemical/mechanical exchange mechanism. Water determines both ion selectivities(8, 27, 30, 31) and exchange rates, which are orders of magnitude slower in anhydrous phlogopites(11) and illites(32) than in hydrated smectites.(33) A striking finding of this work is that layer collapse is significantly slower than the replacement of potassium for sodium by diffusion within the interlayer. A simulation of potassium diffusion at $r = 1$ using the measured layer size distribution shows that complete intercalation is expected to occur in less than a millisecond (SI Appendix) while collapse occurs on the timescale of seconds. It is important to note that anions are excluded from the interlayer in the crystalline swelling regime(34) and are not explicitly considered.

The initial, transient regime of collapse from a uniform population of three-water-layer Na-MMT immediately following mixing provides crucial insight into the dynamic equilibration process. Both the rate and extent of collapse are largely invariant with temperature (SI Appendix), which is consistent with the non-Arrhenian cation diffusion previously observed for MMT,(13, 35) but inconsistent with other processes that could be proposed to limit collapse. We propose that diffusional demixing within the interlayer is the first step in the process of collapse, both in the initial transient regime and during the subsequent period of dynamic equilibrium, and is promoted through positive feedback(36) between the local chemical composition and the interlayer spacing (Fig. 4).

Dynamic fluctuations of MMT interlayers, in which the composition, hydration state, and basal spacing are all tightly coupled, must be common and an important aspect of ion-driven swelling and collapse. Differences in hydration energy between two- and three-water-layer hydrates are 0-4 kT/unit cell of clay, with barriers of comparable size in between,(8, 26, 27) suggesting that both states are regularly explored in fluctuations from the average basal spacing.(37) These fluctuations may present the continually changing migration barriers responsible for non-Arrhenian diffusion.(38) Direct measurements of interlayer spacings in cryo-TEM (Fig. 3c, f, h) exhibit standard deviations of approximately 15%, or ~ 2 -3 Å, consistent with regular exploration of both hydration states with a barrier of ~ 2 -3 kT between them. Because these fluctuations are on the same energy scale as the binding selectivity,(8, 27, 30, 31) these processes must be tightly coupled.

Based on the foregoing evidence, we propose a mechanism of collapse outlined in Fig. 4. Ion intercalation into initially homoionic Na-MMT (Fig. 4a-b) is rapid but

collapse is not immediate (Fig. 4c-d). As the composition in the interlayer equilibrates with the surrounding solution, potassium diffuses throughout the basal surface of the MMT layer, and collapse is initiated by demixing within an interlayer. Demixing promotes potassium colocalization across both sides of an interlayer (Fig. 4e-f), eventually reaching a sufficient size to overcome fluctuations and initiate collapse. Once an interlayer collapses, neighboring layers can be expanded or collapsed,(36) promoting a cascade of individual exchange and hydration/dehydration reactions that lead to demixing of the entire particle. In some cases layers can be liberated through delamination, and may then rotate into preferred rotational configurations via Brownian motion (Fig. 4g-h).

Impact on clay structures. MMT layers can stack with mica-like crystallographic order at relative orientations of only 0 or 180° degrees. However, at relative particle rotations of $\sim 60^\circ$, neighboring particles can come into near-crystallographic alignment along the $\langle 110 \rangle$, $\langle \bar{1}10 \rangle$, $\langle 100 \rangle$ directions. It has long been known that in the initial steps of illitization, mica-like stacking order develops after repeated wetting and drying cycles in the presence of potassium(39) resulting in this type of near-crystallographic ordering.(40) This is the first demonstration that the emergence of this order first arises in suspension as a result of phase separation following potassium exchange, and is maintained across up to 6 Å (two molecular layers) of water. Bending moduli of individual clay layers vary with crystallographic orientation,(41) and thus, (nearly)-oriented layers are expected to be more rigid and less susceptible to perturbations through fluctuations, preserving their relative orientations.

The cooperative process of ion exchange and collapse is a clear demonstration that nanoscale chemical-mechanical coupling controls both the rate and products of ion exchange and the structures that result from collapse in hydrated MMT. This new understanding of exchange equilibria in which multiple swelling states are present will improve the predictive capacity of exchange models of ion binding in swelling clays. We show, for example, that a composition-phase diagram can be used to predict the coexistence of distinct swelling states, and thus the exchange selectivity, of the crystalline hydrates. We demonstrate that the reaction rate is largely unaffected by temperature, but that swelling and collapse hysteresis, a widely observed phenomenon in natural systems, can be attributed to the decreasing collapse rate.

Materials and Methods

Materials. Wyoming montmorillonite (SWy-2), obtained from the Source Clays Repository of The Clay Minerals Society (http://www.clays.org/sourceclays_data.html),

was used throughout this study. Aqueous solutions of NaCl and KCl were prepared from reagent-grade salts.

Static X-ray scattering. X-ray scattering was performed at beamline 5ID-D of the Advanced Photon Source at Argonne National Laboratory in order to obtain high photon fluxes necessary for time-resolved experiments. Small-, medium-, and wide-angle X-ray scattering (SAXS/MAXS/WAXS) was collected simultaneously on three Rayonix charge-coupled device (CCD) detectors with sample–detector distances of 8505.0, 1012.1, and 199.5 mm, respectively. The wavelength of radiation was set to 1.2398 Å (10 keV), resulting in a continuous range of scattering vector, $q = 0.017\text{--}4.2 \text{ \AA}^{-1}$. Additional details are given in the SI Appendix.

Cryo-transmission electron microscopy. Suspensions of Na-MMT or K-MMT with particle concentrations of 5 mg/mL were deposited as 2-3 μL aliquots onto 300-mesh lacy carbon Cu grids (Electron Microscopy Sciences) which had been glow-discharged in air plasma for 15 seconds. Excess solution was removed by automatic blotting (1 blot for 10 s, blot force 10 at 100% relative humidity) before plunge-freezing in liquid ethane using an automated vitrification system (FEI Vitrobot). Imaging was performed with a Titan Krios TEM operated at 300 kV, equipped with a BIO Quantum energy filter. Images were recorded on a Gatan K2 IS direct electron detecting camera with a pixel size of 0.72 Å/pixel. Imaging was performed under cryogenic conditions using a low electron dose rate ($< 10 \text{ e}^-\text{\AA}^{-2}\text{s}^{-1}$) to minimize sample damage. Acquisition was automated with SerialEM software.

Acknowledgements

This research was supported by the U.S. Department of Energy, Office of Science, Office of Basic Energy Sciences, Chemical Sciences, Geosciences, and Biosciences Division, through its Geoscience program at LBNL under Contract DE-AC02-05CH11231. Portions of this work were performed at the DuPont-Northwestern-Dow Collaborative Access Team (DND-CAT) located at Sector 5 of the Advanced Photon Source (APS). DND-CAT is supported by Northwestern University, E.I. DuPont de Nemours & Co., and The Dow Chemical Company. This research used resources of the Advanced Photon Source, a U.S. Department of Energy (DOE) Office of Science User Facility operated for the DOE Office of Science by Argonne National Laboratory under Contract No. DE-AC02-06CH11357. Data was collected using an instrument funded by the National Science Foundation under Award Number 0960140. Access to the FEI Titan Krios was provided through the BACEM UCB facility, and we thank Dan Toso and Elizabeth A. Montabana for technical assistance.

References

1. Hochella MF, Jr., *et al.* (2019) Natural, incidental, and engineered nanomaterials and their impacts on the Earth system. *Science* 363(6434).
2. Bourg IC & Ajo-Franklin JB (2017) Clay, Water, and Salt: Controls on the Permeability of Fine-Grained Sedimentary Rocks. *Acc Chem Res* 50(9):2067-2074.
3. Alt-Epping P, *et al.* (2014) Benchmark reactive transport simulations of a column experiment in compacted bentonite with multispecies diffusion and explicit treatment of electrostatic effects. *Computational Geosciences* 19(3):535-550.
4. Norrish K (1954) The Swelling of Montmorillonite. *Nature* 1:120-134.
5. Tester CC, Aloni S, Gilbert B, & Banfield JF (2016) Short- and Long-Range Attractive Forces That Influence the Structure of Montmorillonite Osmotic Hydrates. *Langmuir* 32(46):12039-12046.
6. Weigand SJ & Keane DT (2011) DND-CAT's new triple area detector system for simultaneous data collection at multiple length scales. *Nuclear Instruments and Methods in Physics Research Section A: Accelerators, Spectrometers, Detectors and Associated Equipment* 649(1):61-63.
7. Moore DM & Robert C. Reynolds J (1997) *Xray diffraction and the identification and analysis of clay minerals* (Oxford University Press, New York, New York) 2 Ed.
8. Liu XD & Lu XC (2006) A thermodynamic understanding of clay-swelling inhibition by potassium ions. *Angew Chem Int Ed Engl* 45(38):6300-6303.
9. Chang F-RC, Skipper NT, & Sposito G (1998) Monte Carlo and Molecular Dynamics Simulation of Electrical Double-Layer Structure in Potassium-Montmorillonite Hydrates. *Langmuir* 14:1201-1207.
10. Ferrage E (2005) Investigation of smectite hydration properties by modeling experimental X-ray diffraction patterns: Part I. Montmorillonite hydration properties. *American Mineralogist* 90(8-9):1358-1374.
11. Sánchez-Pastor N, Aldushin K, Jordan G, & Schmah WW (2010) $\text{K}^+\text{-Na}^+$ exchange in phlogopite on the scale of a single layer. *Geochimica et Cosmochimica Acta* 74(7):1954-1962.
12. Bourg IC & Sposito G (2010) Connecting the Molecular Scale to the Continuum Scale for Diffusion Processes in Smectite-Rich Porous

- Media. *Environmental Science and Technology*(44):2085-2091.
13. Zheng Y & Zaoui A (2013) Temperature effects on the diffusion of water and monovalent counterions in the hydrated montmorillonite. *Physica A* 392:5994-6001.
 14. Rotenberg B, *et al.* (2007) Water and ions in clays: Unraveling the interlayer/micropore exchange using molecular dynamics. *Geochimica et Cosmochimica Acta* 71:5089.
 15. Ho TA, Criscenti LJ, & Greathouse JA (2019) Revealing Transition States during the Hydration of Clay Minerals. *J Phys Chem Lett*:3704-3709.
 16. Eberl D (1980) Alkali cation selectivity and fixation by clay minerals. *Clays and Clay Minerals* 28(3):161-172.
 17. Laird DA & Shang C (1997) Relationship between cation exchange selectivity and crystalline swelling in expanding 2:1 phyllosilicates. *Clays and Clay Minerals* 45(5):681-689.
 18. Wada N, Hines DR, & Ahrenkeil SP (1990) X-ray-diffraction studies of hydration transitions in Na vermiculite. *Physical Review B* 41(8):12895.
 19. Silva GJd, Fossum JO, DiMasi E, & Måløy KJ (2003) Hydration transitions in a nanolayered synthetic silicate: A synchrotron x-ray scattering study. *Physical Review B* 67:094114.
 20. Cases JM, *et al.* (1992) Mechanism of Adsorption and Desorption of Water Vapor by Homoionic Montmorillonite. 1. The Sodium-Exchanged Form. *Langmuir* 8:2730-2739.
 21. Laffer B, Posner A, & Quirk J (1966) Hysteresis in the Crystalline Swelling of Montmorillonite. *Clay Minerals* 6:311.
 22. Berend I, *et al.* (1995) Mechanism of adsorption and desorption of water vapor by homoionic montmorillonites: 2. the Li⁺, Na⁺, K⁺, Rb⁺, and Cs⁺-exchanged forms. *Clays and Clay Minerals* 43(3):324-336.
 23. Vieillard P, Blanc P, Fialips CI, Gailhanou H, & Gaboreau S (2011) Hydration thermodynamics of the SWy-1 montmorillonite saturated with alkali and alkaline-earth cations: A predictive model. *Geochimica et Cosmochimica Acta* 75(19):5664-5685.
 24. Teich-McGoldrick SL, Greathouse JA, Jove-Colón CF, & Cygan RT (2015) Swelling Properties of Montmorillonite and Beidellite Clay Minerals from Molecular Simulation: Comparison of Temperature, Interlayer Cation, and Charge Location Effects. *Journal of Physical Chemistry C* 119:20880-20891.
 25. Holmboe M & Bourg IC (2013) Molecular Dynamics Simulations of Water and Sodium Diffusion in Smectite Interlayer Nanopores as a Function of Pore Size and Temperature. *The Journal of Physical Chemistry C* 118(2):1001-1013.
 26. Whitley HD & Smith DE (2004) Free energy, energy, and entropy of swelling in Cs⁻, Na⁻, and Sr-montmorillonite clays. *J Chem Phys* 120(11):5387-5395.
 27. Tambach TJ, Bolhuis PG, Hensen EJM, & Smit B (2006) Hysteresis in Clay Swelling Induced by Hydrogen Bonding: Accurate Prediction of Swelling States. *Langmuir* 22:1223-1234.
 28. Heinz H, Vaia RA, & Farmer BL (2006) Interaction energy and surface reconstruction between sheets of layered silicates. *The Journal of Chemical Physics* 124(224713):1.
 29. Sposito G (1972) Thermodynamics of swelling clay-water systems. *Soil Science* 114(4):243-249.
 30. Rotenberg B, Morel J-P, Marry V, Turq P, & Morel-Desrosiers N (2009) On the driving force of cation exchange in clays: Insights from combined microcalorimetry experiments and molecular simulation. *Geochimica et Cosmochimica Acta* 73(14):4034-4044.
 31. Teppen BJ & Miller DM (2006) Hydration Energy Determines Isovalent Cation Exchange Selectivity by Clay Minerals. *Soil Science Society of America Journal* 70(1).
 32. Ruiz Pestana L, Kolluri K, Head-Gordon T, & Lammers LN (2017) Direct Exchange Mechanism for Interlayer Ions in Non-Swelling Clays. *Environ Sci Technol* 51(1):393-400.
 33. Arndt D, Mattei M, Heist C, & McGuire A (2017) Measurement of Swelling of Individual Smectite Tactoids In Situ Using Atomic Force Microscopy. *Clays and Clay Minerals* 65(2):92-103.
 34. Tournassat C, Bourg I, Holmboe M, Sposito G, & Steefel C (2016) Molecular Dynamics Simulations of Anion Exclusion in Clay Interlayer Nanopores. *Clays and Clay Minerals* 64(4):374-388.
 35. S. Balme, M. Kharroubi, A. Haouzi, & Henn F (2010) Non-Arrhenian Ionic dc Conductivity of Homoionic Alkali Exchanged Montmorillonites with Low Water Loadings. *Journal of Physical Chemistry C* 114:9431-9438.
 36. Schaettle K, Ruiz Pestana L, Head-Gordon T, & Lammers LN (2018) A structural coarse-grained model for clays using simple iterative Boltzmann inversion. *J Chem Phys* 148(22):222809.

37. Suter JL, Coveney PV, Greenwell HC, & Thyveetil M-A (2007) Large-Scale Molecular Dynamics Study of Montmorillonite Clay: Emergence of Undulatory Fluctuations and Determination of Material Properties. *Journal of Physical Chemistry C* 111:8248-8295.
38. Druger S (1993) Ionic transport in polymer electrolytes based on renewing environments. *Journal of Chemical Physics* 100(5):3979-3984.
39. Plançon A, Besson G, Tchoubar C, Gaultier JP, & Mamy J (1979) Qualitative and Quantitative Study of a Structural Reorganization in Montmorillonite After Potassium Fixation. *Developments in Sedimentology* 27:45-54.
40. Srodon J & Eberl D (1984) Illite. *Reviews in Mineralogy and Geochemistry* 13(1):495.
41. Honorio T, Brochard L, Vandamme M, & Lebee A (2018) Flexibility of nanolayers and stacks: implications in the nanostructuring of clays. *Soft Matter* 14(36):7354-7367.

Figure 1. Static X-ray scattering from Na-MMT and K-MMT. (a, d) Whole-pattern SAXS/MAXS/WAXS fitting. (b, e) Electron density profiles calculated from MAXS diffraction peaks (red) or integrated TEM image contrast (black, one standard deviation in gray). (c, f) Atomic models depicting the structures inferred from the electron density profiles (interlayer water not explicitly shown). Note that cation occupancy is fixed by the structural charge of the layers.

Figure 2. Collapse dynamics during ion exchange between KCl (1 M) and Na-MMT. (a) Time dependence of the extent of collapse, $f(t)$. (b) Stacked SAXS intensity curves showing the emergence of a 2-layer hydrate peak at $q = 0.395 \text{ \AA}^{-1}$ (15.9 \AA) as a function of time after mixing. All samples reach a regime of chemical (ion exchange) and mechanical (layer collapse) equilibrium within 1-2 s. (c) Composition phase diagram. Red circles represent experimental conditions reported in this study.

Figure 3. Low-dose high resolution cryo-TEM of MMT. (a) Na-MMT particle, viewed edge-on. (b) K-MMT particle aligned along high-symmetry zone axes. (c-g) Enlarged portions of (b) corresponding to the top, middle, and bottom layers, respectively, and atomic models that are consistent with image contrast (arrows are the same length. K:orange, Si:blue, Al:teal, other atoms not shown for clarity).

Figure 4. Model of ion exchange and collapse. (a) Edge-on view of initial turbostratic stacking of three layers in Na-MMT. (b) Hypothetical distribution of sodium in proximity to the top of the middle layer, viewed face-on. (c-d) Exchange of potassium for sodium that proceeds prior to collapse. (e-f) Partial collapse induced by critical local potassium concentration. (g-h) Collapse propagates throughout the interlayer, expelling sodium and a single layer of water. Layers dynamically delaminate and restack.